ISSN: 1813-4890

Research and engineering application of full-section fog screen dust capture technology in return airway

Qiaodong Zhang *, Jinwei Qiu

Anhui University of Science and Technology, Huainan City, Anhui Province, China

Abstract

In this study, we developed a full-section fog screen dust capture system installed in the return airway of a comprehensive mining face, aiming to mitigate the pollution generated by dust overflowing from the return airway section during mining. Various spray nozzles were selected to control atomisation under different water pressures. A porous media model was employed to simulate the dust-catching network considering its viscous drag coefficient (D) and inertial drag coefficient ($C_{\_2}$). In addition, changes in pressure drop and the wind loss of the dust-catching network with the wind speed were investigated. Based on a full-size comprehensive mining face model, the atomisation and wind flow field of the full-section fog screen dust capture system were simulated, and the effects of the atomisation degree of droplets from dust capture nets with different apertures on the wind flow field were investigated. The results showed that the optimal spray nozzle was the fan-shaped atomizing spray nozzle, with a selected water pressure of 0.6 MPa. The droplet concentration in the porous media section increased from 0.026 kg/m³ to 0.052 kg/m³, and the volume share increased from 51.5 % to 74.5 %. The concentration of the filtered droplet increased from 0.00067 kg/m³ to 0.0013 kg/m³, and the size of particles adsorbed by the porous media increased from 140 μm in the proportion of most particles to 0.0013 kg/m³. The proportion of most particles above 140 μm was reduced to 0-80 μm, and the optimal pore size was selected to be 100 mu.

Keywords

Spray pressure; Porous media; Dust catchers; Wind flow field; Dust removal.

1. Introduction

Currently, coal plays a crucial role in global energy applications, and China is recognized as a major coal producer. However, the extraction of coal from underground seams necessitates mining operations that inevitably result in elevated levels of coal dust and mixed dust, posing significant health risks to miners.[1,2,3] By the end of 2021, China had reported a total of 1,025,000 cases of occupational diseases. Among them, approximately 915,000 cases (accounting for around 89.3%) were attributed to occupational pneumoconiosis, with over 50% originating from coal mine employees. There are over 100 million workers exposed to dust in China, with 3.473 million employed in the coal industry. Nevertheless, only 3.5% of the coal mine dust employees suffer from pneumoconiosis, despite its prevalence accounting for more than 50% of new cases annually. From 2008 to 2021, approximately 288,000 new reported cases of pneumoconiosis are projected to be reported in China, with coal workers' pneumoconiosis accounting for approximately 120,000 cases (41.7% of all new pneumoconiosis cases). Since 2008, there has been a consistent annual increase in the number of newly reported cases of coal workers' pneumoconiosis in China. Additionally, approximately 1,900 occur each year in national coal mines due to pneumoconiosis, which is six times higher than the number of deaths from coal mine accidents. Coal mine dust has emerged as the primary factor jeopardizing production safety and occupational health, as depicted in Fig. 1.[4-10]

ISSN: 1813-4890

Due to the limited efficiency of simple ventilation dust removal, coal bed water injection, and spray dust removal, the impact of respiratory dust on production safety is significant.[11-13] Composite wet dust removal technology is widely used in fully mechanised mining faces, such as dust suppressants and wetting agents.[14,15] This technology effectively improves the effect of dust removal but presents challenges such as high cost and pollution of coal sources. In recent years, the wet filter dust collector (WFDC) has been progressively developed and implemented. Numerous scholars have studied the mechanism of dust removal. However, their studies mainly focus on the physical relationship between droplets and metal-based filter screens (MBFS) and the effect of sliding behaviour. Suetal.[16] investigated the flow behaviour of droplets impinging on metal screens with varying wettability. The results showed that when impinging on the more hydrophobic wire mesh, smaller and more uniformly distributed secondary droplets were produced. Soto et al.[17] analysed the impact of a droplet on a fine-opening wire mesh and its dispersion process. The results demonstrated that the passage of a droplet through the wire mesh results in the formation of a conical dispersion angle, primarily influenced by side-wall interactions. Ryu et al.[18] investigated the osmotic behaviour of droplets impinging on a fine filament network with two types of surface wettability: hydrophobic and superhydrophobic. Venkateshan et al.[19] analysed the effect of different hydrophobic metal meshes on the sliding of droplets on their surfaces and discovered that the sliding angle of the droplets increased with an increase in the diameter of the filaments.

In recent years, numerical modelling has been extensively used in engineering projects. Wen et al.[20] found that by optimising the relative positions of the pressure tube and the extraction tube and adjusting the extraction pressure ratio, the diffusion and deposition of dust could be effectively reduced. Hua et al.[21,22] analysed the spatial and temporal evolution of dust pollution caused by two typical ventilation methods (blower ventilation and long compression short suction) using FLUENT numerical simulation. Ren et al. [23] designed a novel spraying system based on the dust diffusion behaviour, which was equipped with four nozzles on each side of the classifier. The installation scheme of different nozzles was optimised by numerical simulation. Zhai et al.[24] proposed a multi-nozzle spraying apparatus mounted on the rocker arm of a coal miner to investigate the atomisation mechanism of the nozzles. The instrument exhibited a larger spray coverage, and the optimised spray area improved the suppression efficiency of total and respirable dust by 8%. Qiu et al. [25] investigated the relevant factors of water film formation through numerical simulation and experimental tests. The dust removal mechanism of the full-section fog screen dust capture network was researched, and the dust pollution problem of the roadway was solved by reducing the dust in the return airway of the working face. Although the above studies have effectively addressed the issue of dust removal, the impact of dust removal equipment and the operation of the wind flow in the mine remained unclear.

Hongliulin coal mine north has a plate area with the 25212 comprehensive mining face. The section is rectangular with dimensions of 6.1 m (width) × 4.2 m (height), resulting in a section area of 25.62 m^2. In the wind tunnel, the airflow rate is measured at 2575 m^3/min, with a wind speed of 1.68 m/s. Additionally, the average dust concentration back to the wind tunnel is 34.00 mg/m^3, and the average respiratory dust concentration is 10.37 mg/m^3. The dust concentration in the return airway exceeds the mine safety regulations of 4.0 mg/m^3 and 2.5 mg/m^3, making it challenging to effectively address the issue of dust pollution using conventional methods. Through experiments and simulations, this study investigates the influence of the structure of the dust-catching net and other parameters on the dust reduction method in the return airway. Subsequently, we propose a full-section fog screen dust capture system that enhances dust-removal efficiency while ensuring the normal operation of the tunnel wind flow field.

ISSN: 1813-4890

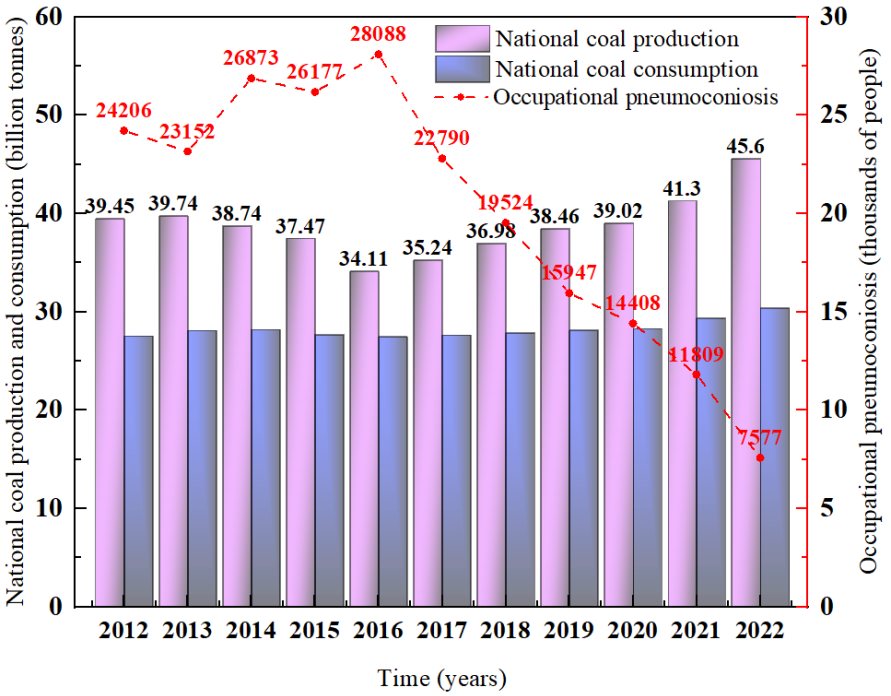

Fig.1. China's national coal production and consumption and occupational pneumoconiosis statistics in recent years

2. Theoretical study of a full cross-section fog screen dust capture system

2.1. Mechanism of water film dust removal

The core part of the full cross-section fog screen dust capture system is the continuous formation of the water film between the fibre filaments, which are constantly disrupted. Under disturbed wind flow, the water film of the dust catcher is the dynamic water film that continuously falls after droplet collisions with the string fence.[26,27] In turn, the capture of dust is realised. The morphology and scale of the droplets after colliding with the grating are primarily affected by the contact angle, and the surface of the grating can be hydrophobic or hydrophilic.[28-34] Due to dynamic water film, the trajectory of dusty airflow passing through the string fence section undergoes constant changes. When the airflow bypasses the water film section of the string fence, it does not strictly adhere to the scientific properties of cylindrical bypassing. The breakage of the water film is affected by various factors, such as filtering wind speed, fibre spacing, and droplet size. The nozzle generates droplets under a certain water pressure, where some smaller droplets pass directly through the gaps between the fibre filaments of the string fence. Meanwhile, another part of the relatively large particle droplets will collide with the fibre filaments. The collision between the droplets and the fibre filaments induces capillary wetting, resulting in a water film of a certain thickness adhering to the surface of the fibre filaments. After the formation of the water film, the gap in the circulation is suddenly filled with water film. At this time, the rupture of the water film occurs through two distinct mechanisms: one is that the wind has active destructive energy on the windward side of the water film, leading to its rupture; the other mechanism is that after the water film is formed, a greater gravity than the surface tension of the water film leads to its rupture, as shown in Fig. 2.

ISSN: 1813-4890

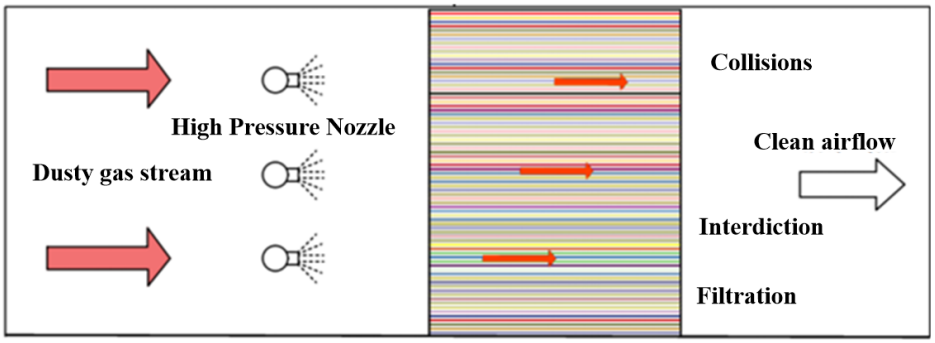

Fig.2. Schematic diagram of dust removal by full cross-section fog screen dust capture system

2.2. Modelling of porous media

In order to simplify the complex dust-catching network geometry, the porous region can be treated as a fluid region with increased drag in fluid calculations. Such treatment usually involves the introduction of a momentum sink in the porous medium related to the fluid velocity to represent the effect of the dust-catching network on the fluid resistance[35,36,37,38]. The momentum sink is usually expressed as follows:

$$S_i = -\left(\sum_{j=1}^{3} D_{ij}\mu v_j \sum_{j=1}^{3} C_{ij}\frac{1}{2}\rho|v|v_j\right) \quad (1)$$

where S_i is the ith (x, y, z) term, which represents the velocity value; D and C are the specified matrices; the first term on the right side of Eq. (1) is the viscous loss term, and the second term is the inertial loss term. Since the screen is a porous medium with uniform distribution, Eq. (1) can be rewritten as:

$$S_i = -\left(\frac{\mu}{\alpha}v_i + C_2\frac{1}{2}|v|v_i\right) \quad (2)$$

where α represents the permeability; C_2 denotes the inertial resistance coefficient. At this point, the matrix D is $1/\alpha$, denoting the viscous drag coefficient. Momentum sinks exert their influence on the fluid to produce a pressure gradient, $\nabla p = S_i$, which can be further expressed as:

$$\nabla p = S_i \Delta n \quad (3)$$

where Δn is the thickness of this porous media basin, i.e., the thickness of the dust-catching mesh.

3. Spray and porous media resistance experiments and validation of effectiveness

3.1. Experimental platform construction

The dust removal efficiency in a fog screen system is closely related to the effect of water film formation on the dust catchers, and the selection of nozzles and dust catchers plays a pivotal role in this process. In this study, the optimal nozzles for the dust-catching net system are selected by setting up the experimental platform for fog screen dust catching, and the resistance of dust-catching nets with different apertures is tested.

The experimental platform of the fog screen dust capture system mainly includes a dust-catching net and spray integrated device, wind, water power system, flow meter, dust sampling device, and particle size analyser (Fig. 3). During the experiment, different mesh filter nets (40 mesh, 80 mesh, 100 mesh, 120 mesh) were tested by adjusting the water pressure size to catch dust net filtration resistance and the distribution of the particle size of the spray.

ISSN: 1813-4890

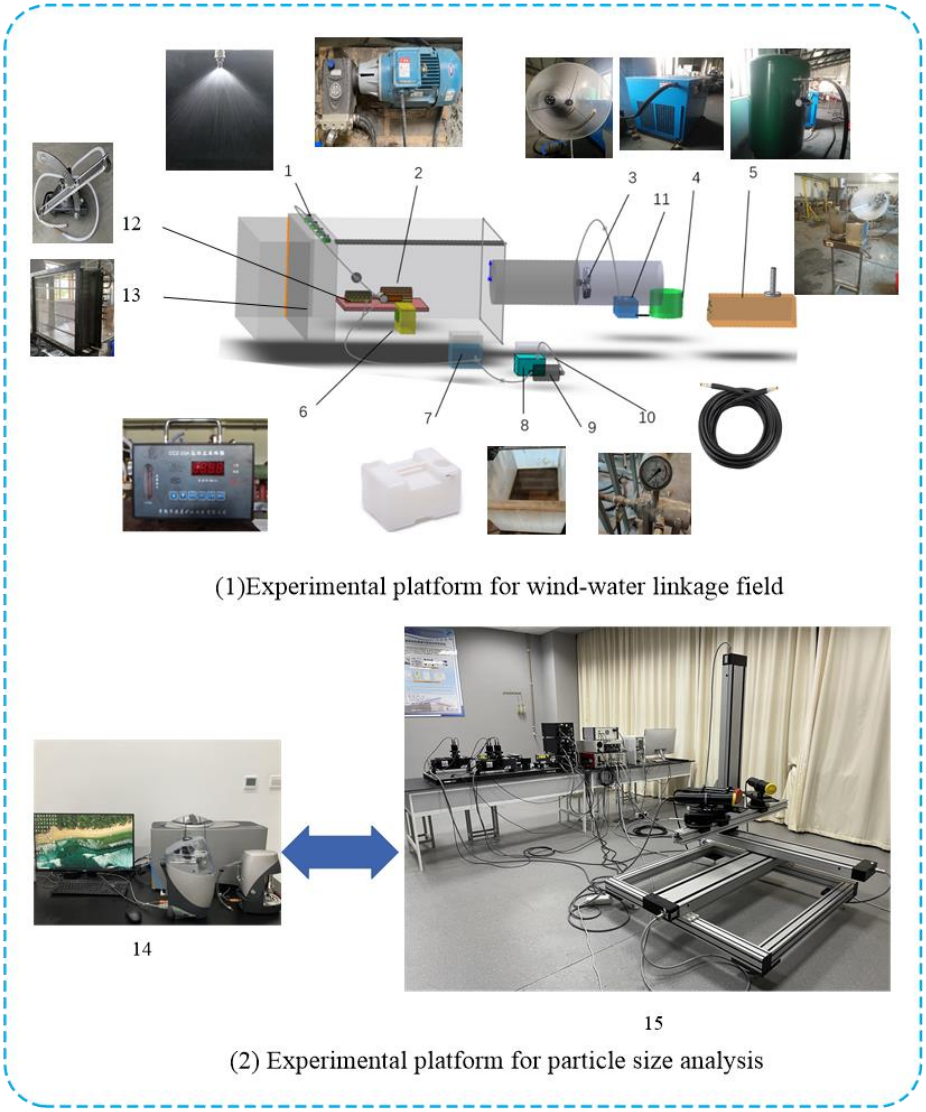

(1)Experimental platform for wind-water linkage field

(2) Experimental platform for particle size analysis

Fig.3. Fog screen dust capture experimental platform

Fig.4. Spray Options

3.2. Nozzle optimisation

In this study, six atomisation nozzles were selected for testing: a guide core containing a flat mouth, a cross-opening hybrid nozzle with an X-shaped guide core, a lateral guide hole centrifugal nozzle, a fine atomisation nozzle, a wide-angle hybrid atomisation nozzle, and a fan-type atomisation nozzle, as shown in Fig. 4. The wind speed under the mine was determined to be 1.65 m/s, and the diameter of the nozzle was 1.1 mm. The atomisation angle in the spray

ISSN: 1813-4890

was tested under different spray pressures, effective ranges, and flow rates, as shown in Table 1.

Table 1 Macro-atomisation parameters for various types of nozzles

Nozzle Type	Spray pressure (MPa)	Fogging angle (°)	Effective range (m)	Flow rate (L/min)
Flat nozzle with deflector core	0.2	56.8	1.8	3.58
	0.4	53.3	2.7	4.63
	0.6	50.6	3.4	5.96
	0.8	48.8	4.2	6.92
Cross-opening mixing nozzles with X-shaped guide core	0.2	87.6	1.9	3.58
	0.4	83.4	2.5	4.86
	0.6	81.2	3.5	5.88
	0.8	78.7	4.4	7.03
Centrifugal nozzles with deflector holes	0.2	72.2	1.3	5.77
	0.4	68.6	1.8	8.12
	0.6	66.0	2.6	9.74
	0.8	64.1	3.4	11.74
Fine Atomisation Nozzles	0.2	46.6	1.2	2.65
	0.4	41.9	1.6	3.80
	0.6	39.8	2.2	4.65
	0.8	36.3	2.8	5.63
Wide angle hybrid atomising nozzles	0.2	51.7	1.5	5.05
	0.4	42.5	1.8	6.50
	0.6	37.3	2.4	7.70
	0.8	34.7	2.7	8.82
Fan Atomising Nozzles	0.2	90.3	3.0	2.33
	0.4	87.6	3.3	2.98
	0.6	85.1	4.1	3.35
	0.8	83.3	4.4	4.45

As can be seen from Table 1, the atomisation angle and effective range of the fine atomisation nozzle and wide-angle hybrid atomisation nozzle are relatively poor compared to the other four nozzles. Therefore, the contact area between the dust and spray field is small, leading to relatively poor film formation and dust removal efficiency. The flat nozzle with a deflector core has a good effective range but poor atomisation angle, while the lateral deflector hole centrifugal nozzle has a wide atomisation angle but a poor effective range, negatively affecting the formation of water film and dust removal effect. The cross-opening hybrid nozzle with an X-shaped deflector core and fan-type atomising nozzle have better atomization angles and effective ranges. Therefore, a particle size analyser was used for further analysis of the atomisation effect of the two types of nozzles (refer to Table 2 for Type I and Type II, which represent the fan-type atomising nozzle and cross-opening hybrid nozzle with X-shaped deflector core, respectively; d_{10}, d_{50}, and d_{90} denote the characteristics of the sizes, including the volume of particles smaller than this size; specifically, they denote the content of 10%, 50%, and 90% of the total particle volume, respectively). It can be concluded that the fan-shaped atomisation nozzle has a small droplet size. For example, when the pressure reaches 0.6 MPa, the atomisation angle of the fan-shaped atomisation nozzle can reach 831, the effective range is up to 4.1 m, d_{10} is 43.5 μm, d_{50} is 108.5 μm, and d_{90} is 190.6 μm. Due to the large space of the

ISSN: 1813-4890

tunnel where the fog screen dust capture system is located, a dust removal net with smaller pores was selected. In order to improve the dust removal effect, sector spray nozzles were selected, which have a wide spray angle, a wide effective range, and small spray particles. As can be seen from Tables 1 and 2, the atomisation angle changes slightly. When the spray pressures are 0.6 MPa and 0.8 MPa, the spray range increases by only 0.3 m, while the flow rate increases to 1 L/min, ultimately increasing the cost of use. As the difference between the two spray particle sizes is small, the spray pressure of 0.6 MPa is selected for the dust removal system.

Table 2 Atomized particle size of nozzle

Types	Water supply pressure(MPa)	Grain size (μm)		
		d_{10}	d_{50}	d_{90}
I	0.2	59.6	129.6	245.4
	0.4	46.8	115.7	219.6
	0.6	43.5	108.5	190.6
	0.8	40.7	101.4	185.8
II	0.2	86.6	166.3	545.8
	0.4	80.3	134.5	435.8
	0.6	66.8	120.4	377.4
	0.8	61.5	106.7	262.3

3.3. Porous media resistance experiment

Four types of 304 stainless steel dust capture meshes are used in this simulation experiment, which are 40 mesh (0.5 mm aperture, 0.13 mm filament diameter), 80 mesh (0.25 mm aperture, 0.09 mm filament diameter), 100 mesh (0.18 mm aperture, 0.08 mm filament diameter), and 120 mesh (0.15 mm aperture, 0.07 mm filament diameter), shown in Fig. 5. Their velocity and pressure drop are tested after the gas passes through the porous media region at velocities (v) of 3 m/s, 5 m/s, 7 m/s, and 9 m/s.

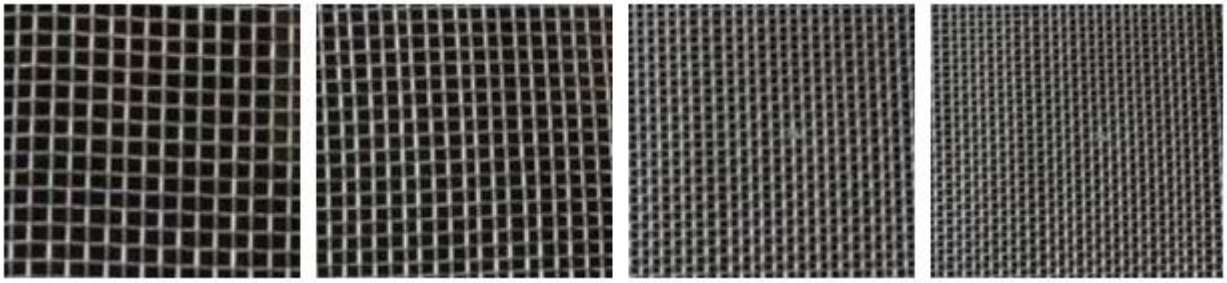

40mu 80mu 100mu 120mu

Fig.5. Filter physical picture

The above figure illustrates a positive correlation between the velocity of the gas after passing through the porous media region and the pressure drop[39], which is fitted according to the above equation. Consequently, an equation representing the relationship between pressure drop and velocity can be derived, as shown in Fig. 6.

$$\Delta p = av^2 + bv \tag{4}$$

As shown in Fig. 6, a higher initial mesh count results in a greater and more uniform pressure drop. As the wind speed v increases, the difference between the pressure drops of different mesh gradually increases. When the speed v reaches 5 m/s, the difference is more obvious. The pressure drop of dust capture mesh is 80 mesh, 40 mesh, 120 mesh, and 100 mesh in

ISSN: 1813-4890

descending order. According to the above formula, the inertial resistance coefficient C_2 and the viscous resistance coefficient D can be obtained, as shown in Table 3.

$$a = C_2 \frac{1}{2} \rho \Delta n \tag{5}$$

$$b = \frac{\mu}{\alpha} \Delta n \tag{6}$$

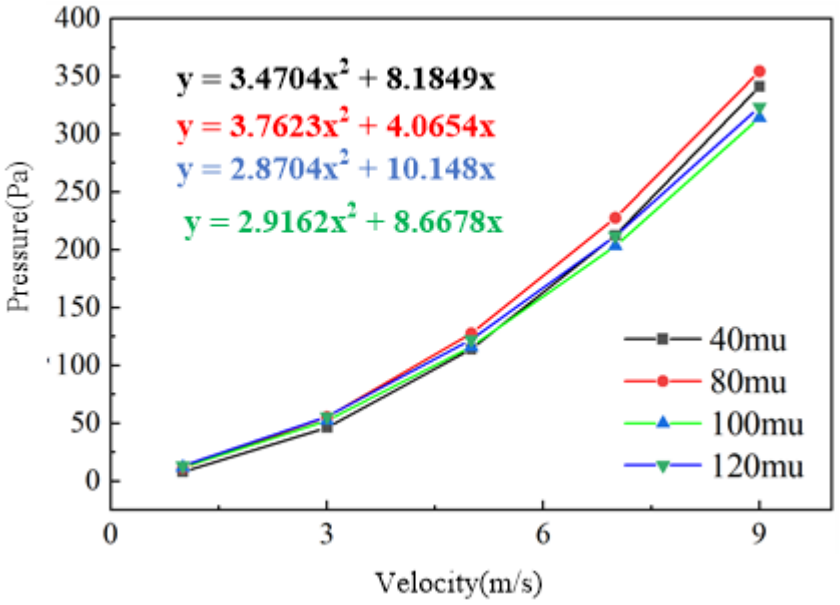

Fig.6. Porous media data fitting diagram

Table 3 Parameters of porous media

Catalogue	a	b	Viscous drag coefficient (D)	Inertial drag coefficient (C_2)
40mu	3.7623	4.0654	47.265	1.7788e+6
80mu	3.4707	8.1849	62.9551	5.1737e+6
100mu	2.9162	8.6678	59.5142	6.1631e+6
120mu	2.8704	10.148	66.9481	1.7788e+6

It can be concluded that the pressure drop and wind loss of the dust catchers increase with increasing wind speed, with a smaller aperture mesh of the dust catchers leading to a more significant pressure drop and wind loss.

3.4. Numerical simulation validation

After measuring the relevant parameters of the spray field, the authenticity and feasibility of the numerical simulation were verified by comparing the experimental platform with the simulation software. The fan speed was set to 1.65 m/s, the 1.1 mm nozzle with a fan-shaped atomising nozzle was selected, and the spray pressure was set to 0.6 MPa. The position of the nozzle was (0, 0.48, -0.5), and the horizontal and vertical directions of the airflow were set to the X-axis and the Y-axis, respectively, as shown in Fig. 7.

ISSN: 1813-4890

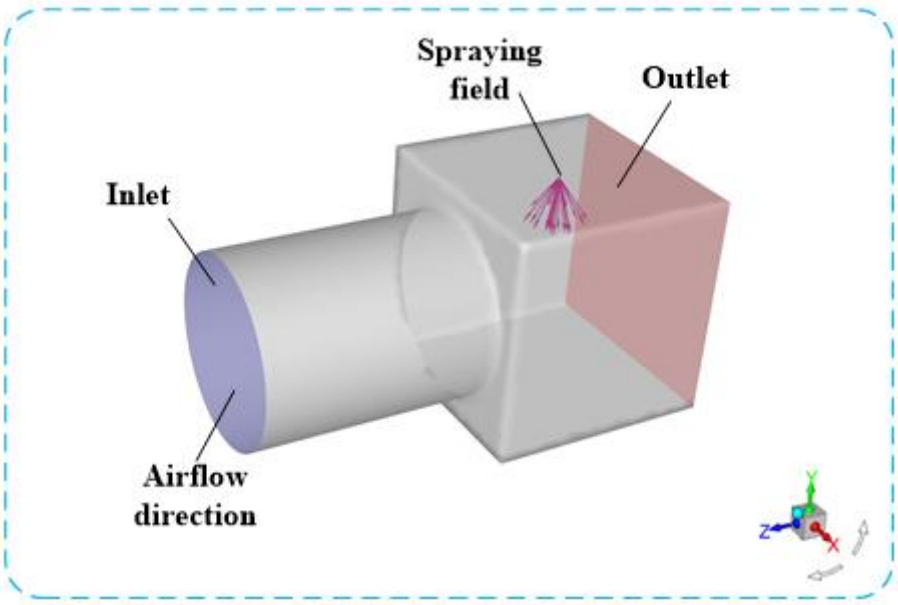

Fig.7. Simulated measurement diagrams in the spraying field

A model that matched the scale of the experimental platform was constructed using SolidWorks software, and the mesh was generated using FLUENT meshing. Subsequently, a numerical simulation of the spray was carried out using FLUENT. The boundary conditions are shown in Table 4 below. Figures 8 and 9 show the simulated spray droplet sizes to determine the simulation feasibility by comparing them with the particle size ratios obtained from the particle size analyser.

Table 4 Parameterisation

Setup	Parameter setting
Gravitational acceleration	9.81m/s^2
Model	k-epsilon(2 eqn)
Inlet	1.65 m/s
Outlet	Pressure outlet
k-epsilon Model	Realizable
Injection Type	Cone
Material	Water - liquid
Min. Diameter (mm)	0.001
Max. Diameter (mm)	0.22
Mean Diameter (mm)	0.1
Solver	Transient

As shown in Figs. 8 and 9, the effect of the airflow on the spray field is consistent in both the spray detail experiments and numerical simulations. Transverse airflow induces a shift of the spray field towards the outlet. The comparison between the experimental and numerical simulation results reveals that the particle size error at each measurement point within the spray field is limited to 3.46%. This result indicates the consistency between the numerical simulation and the results of the fine view experiment, demonstrating the accuracy of the numerical simulation.

ISSN: 1813-4890

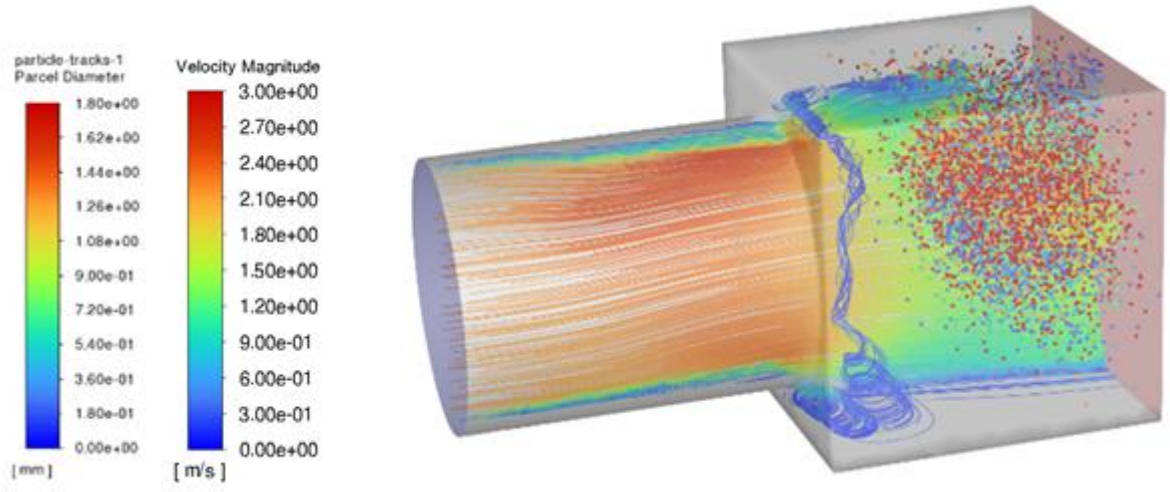

Fig.8. Droplet size in the spray field

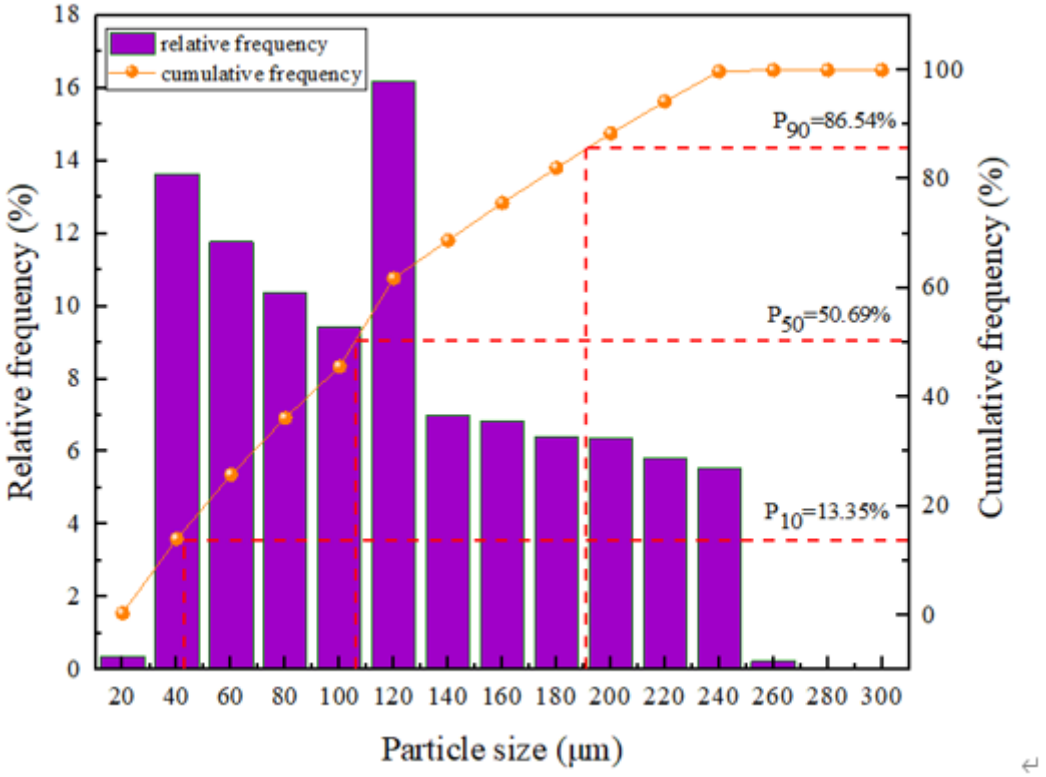

(P_{10}, P_{50}, P_{90} represent the specific gravity at 0.6 Mpa corresponding to the range ofd_{10}, d_{50}, d_{90} particle sizes)

Fig.9. Simulated particle size distribution

4. Spray and porous media resistance experiments and validation of effectiveness

4.1. Modelling

The SolidWorks software was used to establish a local model of the 25212 comprehensive mining face in the Hongliulin North 1 plate area, including the inlet and return alleys (W×H=6.1×4.2 m), a coal miner, and a hydraulic support, as shown in Fig. 10.

ISSN: 1813-4890

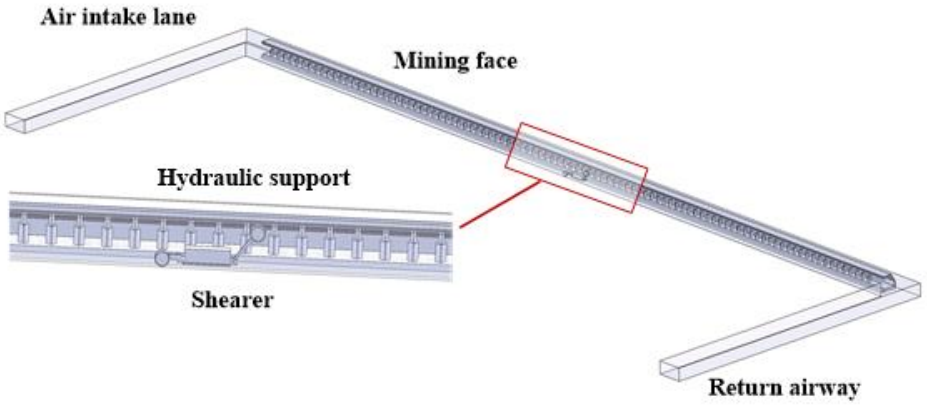

Fig.10. Model of 25212 working face in Hongliulin North 1 plate area

4.2. Meshing

Unstructured meshes are widely applied in meshing for numerical simulation, particularly tetrahedron, which is extremely suitable for delineating irregular and complex geometric models. Along with the continuous development of computer and mesh technology, more and more scholars will use unstructured meshes to divide complex physical models when applying numerical simulation methods.[40,41] This simulation adopts tetrahedral mesh division through FLUENT meshing software, as shown in Fig. 11. The mesh size is 0.03-0.3 m, with a smooth transition in the boundary layer. A total of 184 meshes are employed, the minimum cell mesh quality is 0.32 greater than 0.15, and the maximum distortion degree is 0.65 less than 0.9, which can be used in simulation calculation.

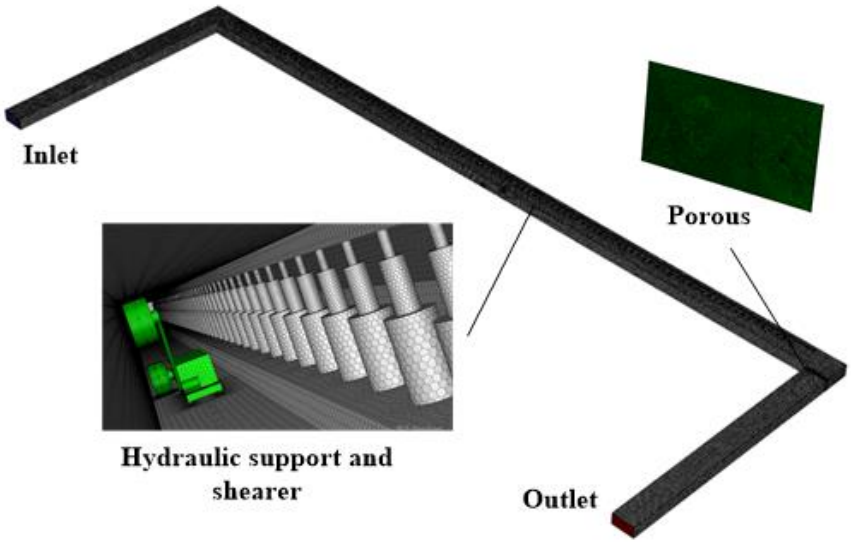

Fig.11. Grid Schematic

4.3. Simulation of water mist effect and particle adsorption in full-section fog screen dust capture system

The meshed model was imported into FLUENT software, the airflow velocity was set to 1.65 m/s, and the spray simulation of the fog screen dust capture system was simulated using fan-shaped atomised nozzles. The water pressure was set to 0.6 MPa, with a total of 11 nozzles spaced at intervals of 0.5 m and an aperture diameter of 1.1 mm for each nozzle. The spraying system was positioned approximately 40 cm away from the fog screen dust capture net, and the water spray effect of the fog screen dust capture system was simulated by the porous media model with different aperture mesh. The other parameters considered in the numerical

ISSN: 1813-4890

simulation of the water mist effect of the fog screen dust capture system are listed in Table 1. On this basis, the distribution patterns of front-end, back-end, and porous media spray fields, as well as cloud diagrams in the section where the collaborative dust-catching network is located, are obtained and presented in Fig. 12 and Table 5. Considering that the porous media region represents a thin fluid domain, we set up the profiles to observe the adsorption of the particles and to calculate the different distributions of particle sizes, as shown in Fig. 13.

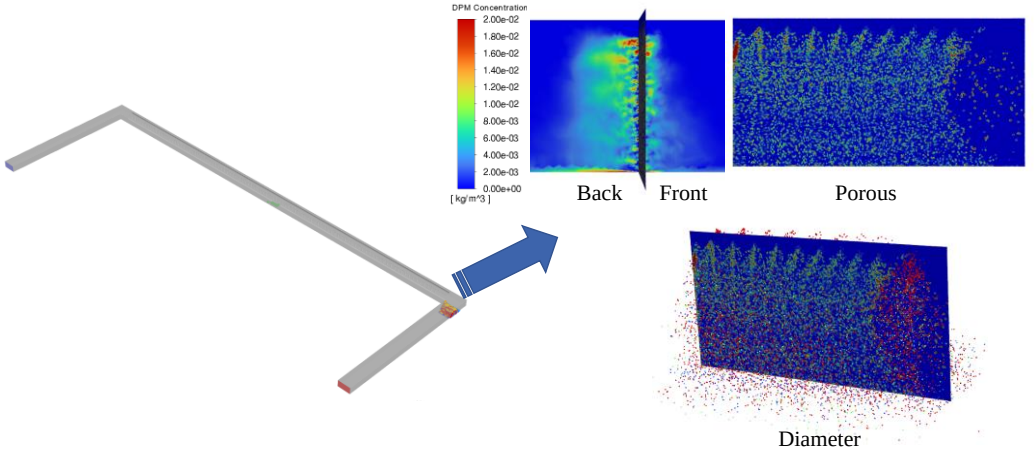

(a) 40mu

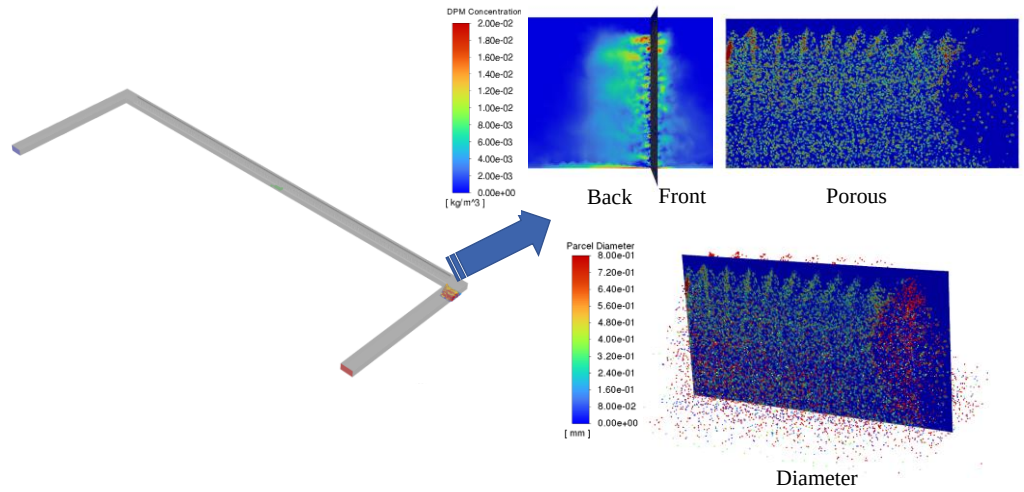

(b) 80mu

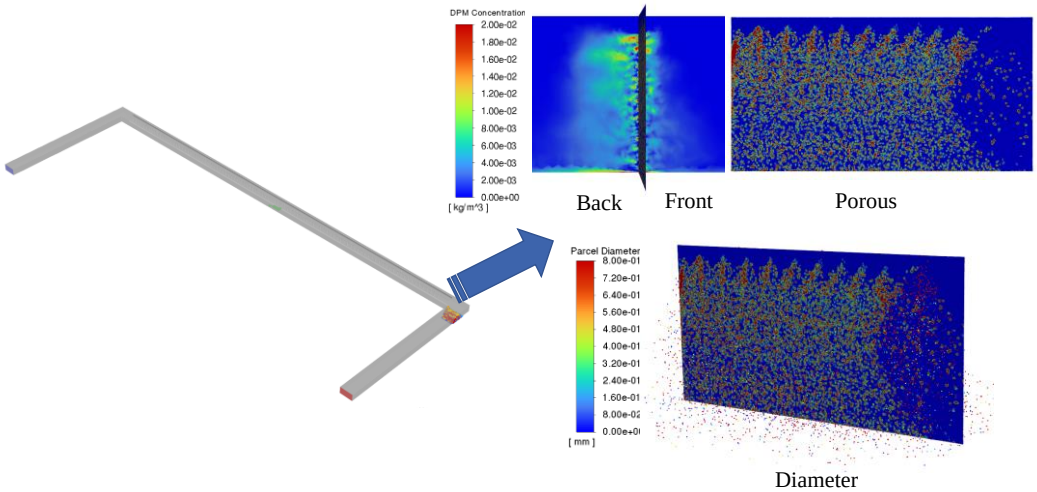

(c) 100mu

ISSN: 1813-4890

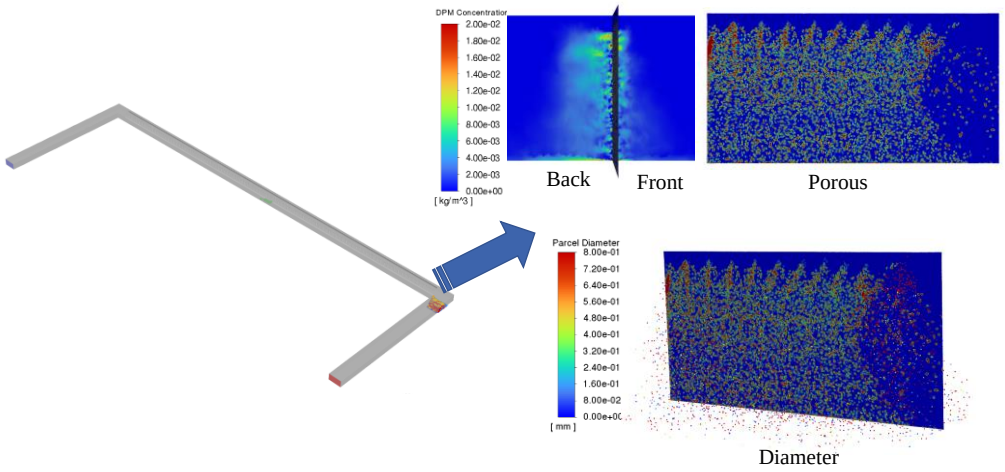

(d) 120mu

Fig.12. Spray field distribution patterns and cloud maps

Table 5 Concentration and proportion of spray field

Name	Front (kg/m³)	Back (kg/m³)	Porous (kg/m³)	Volume ratio(%)
40mu	0.00289	0.00213	0.026	51.5
80mu	0.00292	0.00195	0.039	63.2
100mu	0.00286	0.00156	0.052	74.5
120mu	0.00287	0.00147	0.057	78.9

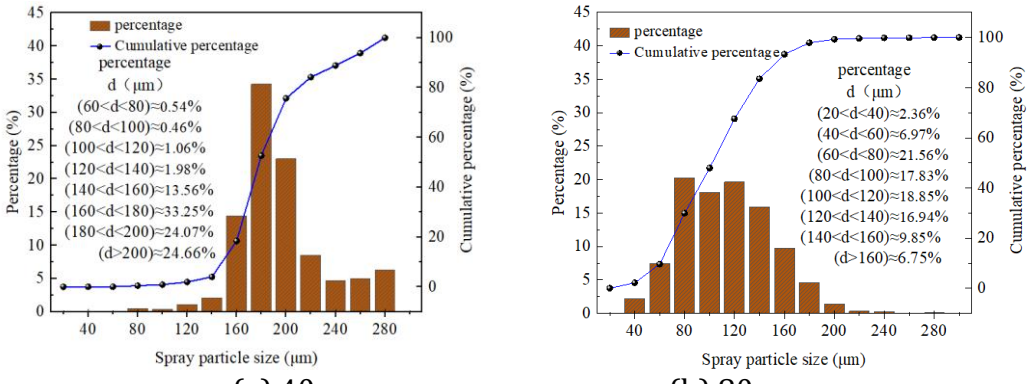

(a) 40 mu

(b) 80 mu

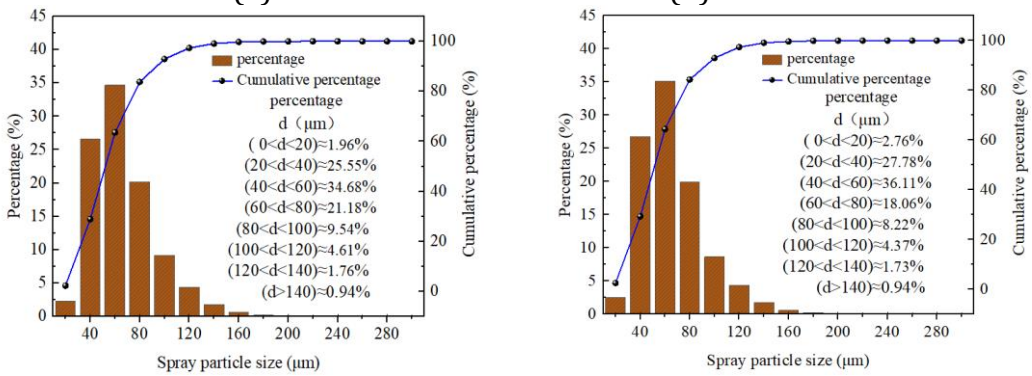

(c) 100 mu

(d) 120 mu

Fig.13. Adsorption ratio of different pore sizes

According to the simulation results (Figs. 12 and 13 and Table 5), the water pressure is 0.6 MPa upon activation of the fog screen dust capture system, increasing the mesh size of the dust capture net from 40 mu to 120 mu. When the aperture is 40 mu, the concentration difference

ISSN: 1813-4890

between the front and back of the net is 0.00067 kg/m^3, the concentration of the porous media part is 0.026 kg/m^3, and the droplet volume share is 51.5%, with the majority of captured droplet sizes being 140 μm or larger. When the pore size is 80 mu, the concentration difference is 0.00097 kg/m^3, the concentration of the porous media part is 0.039 kg/m^3, and the droplet volume accounts for 63.2%, with the majority of captured droplet sizes in the range of 60-140 μm. When the pore size is 100 mu, the concentration difference is 0.0013 kg/m^3, the concentration of the porous media part is 0.052 kg/m^3, and the concentration of the porous media part is 0.0013 kg/m^3. When the mesh size is 100 mu, the concentration difference is 0.0013 kg/m^3, the concentration of porous media is 0.052 kg/m^3, and the droplet volume accounts for 74.5%, with most of the droplet sizes in the range of 0-80 μm. When the mesh size is 120 mu, the concentration difference is 0.0014 kg/m^3, the concentration of porous media is 0.057 kg/m^3, and the droplet volume accounts for 78.9%, encompassing small particles in the range of 0-80 μm. The droplet size distribution in the dust capture system is similar to that of 100 mu, with a slight increase in the proportion of small particles. The droplet concentration and volume of the porous media part increase significantly as the aperture increases from 40 mu to 100 mu. Following the filtration of the dust catcher, the droplet concentration exhibits a significant decrease, accompanied by a rapid increase in the proportion of small particles captured by the porous media section. Eventually, this proportion reaches a stable level at 120 μm.

4.4. Simulation of the flow field of a full cross-section fog screen dust capture system

The full cross-section fog screen dust capture system was arranged in the return airway. When selecting the screen mesh, both the degree of atomisation and the pressure drop (ΔP) and wind loss (ΔV) during the operation were considered, thus minimising the impact on the wind flow under the mine. On this basis, the flow field during its operation was observed, and its wind speed vector diagram and pressure cloud diagram are illustrated in Fig. 14.

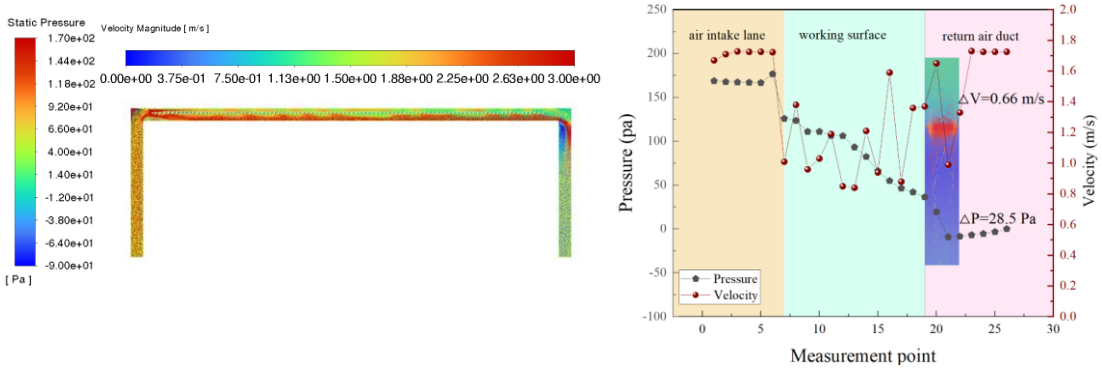

(a)Flow field simulation for an orifice of 40 mu

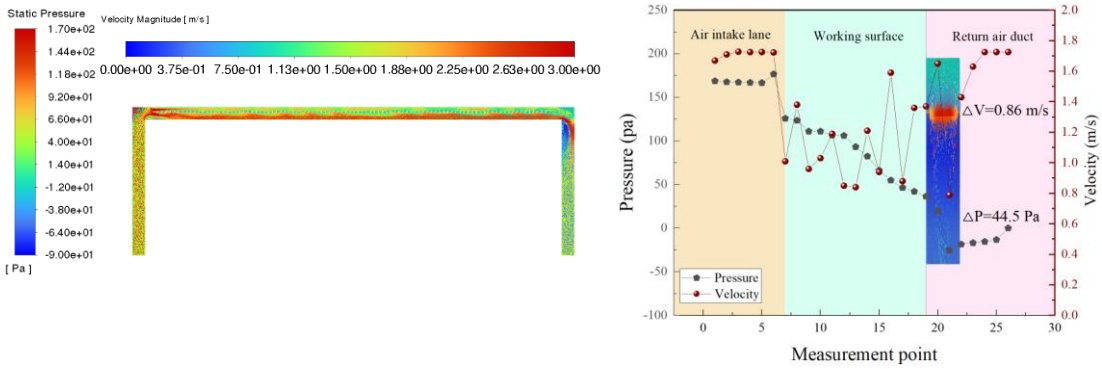

(b)Flow field simulation for an orifice of 80 mu

ISSN: 1813-4890

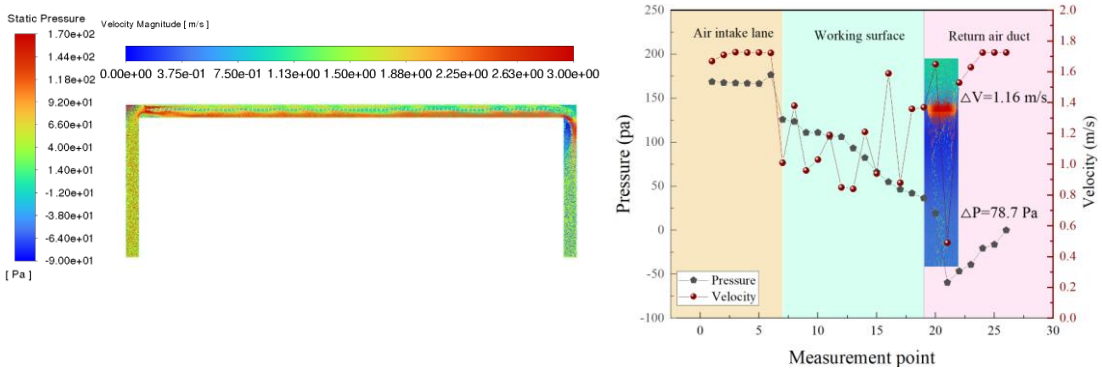

(c)Flow field simulation for an orifice of 100 mu

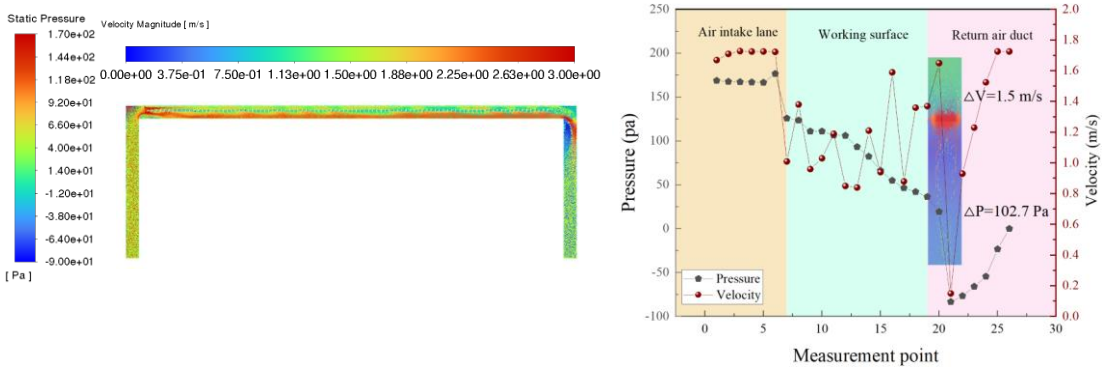

(d)Flow field simulation for an orifice of 120 mu

Fig.14. Simulation and analysis of flow fields at different orifice

According to the flow field simulation results (Fig. 14), the aperture is 40 and 80 mu, the pressure difference is 28.5 and 44.5 Pa, and the wind loss is 0.66 and 0.86 m/s, respectively. The magnitudes of flow field losses were found to be relatively small. When the aperture reaches 100 mu, the pressure is 78.7 Pa, and the wind is 1.16 m/s, with an accelerated increasing rate of the flow field loss. When the aperture reaches 100 mu, the pressure is 102.7 pa, the wind is 1.5 m/s, and the flow field loss value maintains a rapid upward trend. Combined with the above atomisation analysis, for a spray flow rate of 0.6 MPa, the atomisation effect of the 40 mu to 100 mu system becomes more significant, with an increase in the proportion of small particles. Considering the atomisation of the dust removal and the stability of the flow field, the pressure drop and wind loss in the return airway continue to exhibit an increasing trend with a 120 mu aperture. Therefore, a dust catcher of 100 mu mesh can be selected for the full cross-section of the fog screen dust capture system

5. Conclusion

(1)Through multi-characteristic experiments with a full-section fog screen dust capture system, this study analyses the spray field on a macro-scale to optimise the effectiveness of the nozzles in the dust capture system. The fan-shaped nozzle exhibits superior atomization efficiency and provides the widest coverage among the tested nozzles. By maintaining an atomisation pressure of 0.6 MPa, a balance is achieved between cost savings and sustaining optimal atomisation performance. The viscous drag coefficient (D) and inertial drag coefficient (C_2) of different mesh screens in the porous media model are obtained by tilting a micromanometer to calculate differential pressure of mesh at varying wind speeds. When comparing the particle size data of the spray field obtained from the spray experiments with the numerical simulation results, the maximum error of 3.43% is observed, indicating that the results of the spray numerical simulation are basically accurate.

(2)A full-size model of the 25212 comprehensive mining face in the Hongliulin North 1 plate area is established, and the full-section fog screen dust capture system is subjected to a

numerical simulation. The numerical simulation results showed that as the aperture increases from 40 mu to 100 mu, the droplet concentration of the porous media part increases from 0.026 kg/m^3 to 0.052 kg/m^3, and the volume share of the porous media part increases from 51.5% to 74.5%. The droplet concentration of the dust-catching mesh filtered decreases sharply, and the droplet concentration of the filtered droplet increases from 0.00067 kg/m^3 to 0.0013 kg/m^3. The particle size of the adsorbed particles in the porous medium decreases from 140 μm to 0-80 μm and stabilises at 120 mu, indicating that a 100 mu dust catcher is suitable for the full cross-section fog screen dust capture system.

References

[1] Weimin Cheng, Haiming Yu, Gang Zhou, Wen Nie,The diffusion and pollution mechanisms of airborne dusts in fully-mechanized excavation face at mesoscopic scale based on CFD-DEM,Process Safety and Environmental Protection,Volume 104, Part A,2016,Pages 240-253,ISSN 0957-5820,

[2] José A. Aznar-Sánchez, Juan F. Velasco-Muñoz, Luis J. Belmonte-Ureña, Francisco Manzano-Agugliaro,Innovation and technology for sustainable mining activity: A worldwide research assessment,Journal of Cleaner Production,Volume 221,2019,Pages38-54,

[3] Dominik Bałaga, Michał Siegmund, Marek Kalita, Ben J. Williamson, Andrzej Walentek, Marcin Małachowski,Selection of operational parameters for a smart spraying system to control airborne PM10 and PM2.5 dusts in underground coal mines,Process Safety and Environmental Protection,Volume 148,2021,Pages 482-494,

[4] YUAN Liang. Scientific Concept of Coal Mine Dust Prevention and Control and Occupational Safety and Health[J]. Coal Journal，2020,45(1):1-7.YUAN Liang.Scientific conception of coal mine dust control and occupational safety[J].Journal of China Coal Society,2020,45(1):1-7.

[5] CHENG Weimin, ZHOU Gang, CHEN Lianjun, et al. 20-year research progress and prospect of coal mine dust control theory and technology in China[J]. Coal Science and Technology.2020,48(2):1-20.CHENG Weimin,ZHOU Gang,CHEN Lianjun,et al.Research progress and prospect of dust control theory and technology in China'scoal mines in the past 20 years[J].Coal Science and Technology,2020,48(2):1-20.

[6] LI Gang, WU Jiangyou, KIM Yongchul, et al. Research status and outlook of dust prevention technology in metal mines in China[J]. Metal Mining.2021(1):154-167.LI Gang,WU Jiangyou,JIN Longzhe,et al.Study status and prospect of dust control technology for metal mines in China[J].Metal Mine,2021(1):154-167.

[7] G. Xu, E.C. Jong, K.D. Luxbacher, et al. Remote characterization of ventilation systems using tracer gas and CFD in an underground mine[J].Safety Science.74(2015)140-149.

[8] C.Y.Liu,W.Nie,X.F.Liu,Y.Hua,W.W.Zhou,F.N.Yu,et al.Behavior of the particulate matter (PM) emitted by trackless rubber-tyred vehicle (TRTV) at an idle speed under different movement conditions and ventilation optimization[J] Sci Total Environ,783(2021), Article147008,10.1016/ j.scitotenv. 2021. 147008.

[9] Z.Adamis,M.Timár,L.Köfler,et al.Biological effects of the respirable dusts from ore mines[J] Environ Res,41(1986), pp.319-326.

[10] S.M. Liu, W.M. Cheng, G. Wang, L Fan, R Zhang. Special Issue on mine dust research:health effects and control technologies[J]. International Journal of Coal Science & Technology, 2(2021):177-178.

[11] W. Nie, B. Yang, T. Du, H. Peng, X. Zhang, Y. Zhang，Dynamic dispersion and high-rise release of coal dust in the working surface of a large-scale mine and application of a new wet dust reduction technology，J. Clean. Prod., 351 (2022), Article 131356.

[12] C. Xu, W. Nie, Z. Liu, H. Peng, S. Yang, Q. Liu，Multi-factor numerical simulation study on spray dust suppression device in coal mining process Energy, 182 (2019), pp. 544-558.

[13] Q. Zhang, X. Xing, G. Zhou, Y. Hu, S. Shang, M. Fu, H. Ma, H. Li, Y. Men Preparation and micro-wetting mechanism analysis of highly permeable-moistening additive for coal seam water injection based on plant extraction technology，Fuel, 322 (2022), Article 124125.

[14] Gao et al., 2023M.Gao,H.Li,Y.Zhao,Y.Liu,W.Zhou,L.Li,J.Xie,J.Deng Mechanism of micro-wetting of highly hydrophobic coal dust in underground mining and new wetting agent development Int. J. Min. Sci. Technol.,33(2023), pp.31-46.

[15] Wei et al., 2020 X.Wei,H.Wang,Y.Xie,Y.Du An experimental investigation on the effect of carboxymethyl cellulose on morphological characteristics of dust-suppression foam and its mechanism exploration Process Saf. Environ. Prot.,135(2020), pp.126-134.

[16] Suetal., 2020 M.-J.Su,Y.Luo,G.-W.Chu,Y.Cai,Y.Le,L.-L.Zhang,J.-F.Chen Dispersion behaviors of droplet impacting on wire mesh and process intensification by surface micro/nano-structure Chem. Eng. Sci.,219(2020), Article 115593.

[17] Soto et al,2018 D.Soto,H.L.Girard,A.L. Helloco,T.Binder,D.Quéué,K.K.Varanasi,Droplet fragmentation using a mesh Phys. Rev. Fluids,3(2018), p.083602,10.1103/ Phys Rev Fluids. 3.083602.

[18] Ryu et al., 2017S.Ryu,P.Sen,Y.Nam,C.Lee.Water penetration through a superhydrophobic mesh during a drop impact,Phys. Rev. Lett.,118(2017), p.014501,10.1103/PhysRevLett.118.014501.

[19] D.G.Venkateshan,H.V.Tafreshi.Modelling droplet sliding angle on hydrophobic wire screens. Colloids Surf. A: Physicochem. Eng. Asp.,538(2018), pp.310-319

[20] Hu Wen, Wan sheng Mi, Shixing Fan, Yu Xu, Xiaojiao Cheng. Simulation study on crucial parameters of long compressiveand short suction ventilation in large section roadway excavationof LongWangGou coal mine. Environmental science and pollution research international.

[21] Y.Hua,W.Nie,P.Cai,et al.Pattern characterization concerning spatial and temporal evolution of dust pollution associated with two typical ventilation methods at fully mechanized excavation faces in rock tunnels.Powder Technol.,334(2018), pp.117-131.

[22] Y.Hua,W.Nie,Q.Liu,et al.The development and application of a novel multi-radial-vortex-based ventilation system for dust removal in a fully mechanized tunnelling face.Tunn. Undergr. Space Technol.,98 (2020), Article 103253

[23] T.Ren,Z.Wang,G.Cooper.CFD modelling of ventilation and dust flow behaviour above an underground bin and the design of an innovative dust mitigation systemTunn. Undergr. Sp. Technol. Inc. Trenchless Technol. Res.,41(2014), pp.241-254,10.1016/j.tust.2014.01.002.

[24] Q.Zhou,B.T.Qin,F.Wang,H.T.Wang,J.Hou,Z.R.Wang.Effects of droplet formation patterns on the atomization characteristics of a dust removal spray in a coal cutter[J].Powder Technol,344(2019), pp.570-580.

[25] Jinwei Qiu, Qiaodong Zhang, Binyou Jiang, Mingyun Tang, Liang Zhou,Analysis of the effect of water film dust removal of a tunnel's full-section fog screen dust capture system,Chemical Engineering Research and Design,Volume 209,2024,Pages 258-271,ISSN 0263-8762,https:// doi.org/ 10.1016/j. cherd.2024.07.063.

[26] MEAD-HUNETR Ryan,KING Andrew J C,MULLINS Benjamin J.Aerosol-mist coalescing filters:A review[J].Separation and Purification Technology,2014,133:484-506.

[27] MEHDIZADEH S Neda,PASDAR AmirMedsi,CHASE George G.Correlations between air drag and movement of water droplets in fibrous media[J].Separation and Purification Technology, 2021, 267:118602.

[28] AGRANOVSKI Igor E,BRADDOCK Roger D.Filtration of liquid aerosols on wettable fibrous filters[J].Environmental and Energy Engineering,1998,12(44):2775-2783.

[29] WANG Yulei,WANG Yuxiang,WANG Shaorong.Droplet impact on cylindrical surfaces:Effects of surface wettability,initial impact velocity,and cylinder size[J].Journal of Colloid and Interface Science,2020,578:207-217.

[30] WANG Yifei,ZHUANG Dawe,DING Guoliang.Effect of surface wettability of fins on dust removal by condensate water[J].International Journal of Heat and Mass Transfer,2019,190:1260-1271.

[31] ZHANG Jing, ZHANG Yan, LIU Yujian, et al. MWCNTs modified composite superhydrophobic coatings and their chemical resistance[J]. Journal of Materials Science and Engineering. 2020,38(2):250-255.ZHANG Jing,ZHANG Yan,LIU Yujian,et al.MWCNTs modification of super hydrophobic

composite coating with high chemical resistance[J].Journal of Materials Science & Engineering,2020,38(2):250-255.

[32] Xue B, Zhang F, Zhu H, et al. Research progress on long-lasting superhydrophobic nanocomposites [J]. SCIENCE CHINA: Physics Mechanics Astronomy.2018,48(9):54-70.XUE Xiao, ZHANG Hui,ZHU Hongwei,et al.Durable superhydrophobic nanocomposite materials[J]. Scientia Sinica Physica, Mechanica & Astronomica,2018,48(9):54-70.

[33] MIN Fanfei, REN Bao, CHEN Jun, et al. Mechanism and experimental study of promoting coal slurry dewatering based on hydration film weakening[J]. Journal of Coal.2020,45(1):368-376.MIN Fanfei,REN Bao,CHEN Jun,et al.Mechanism and experimental study on promoting coal slime dewatering based on weakening of hydration layer[J].Journal of China Coal Society,2020,45(1):368-376.19202122232425

[34] ZHANG Jing, XU Haibo, HUANG Yue, et al. Preparation and interfacial structure control of bilayer transparent wear-resistant superhydrophobic membrane layer[J]. Materials Herald.2020,34 (12): 12005-12009ZHANG Jing,XU Haibo,HUANG Yue,et al.Preparation and interface structure control of bilayer transparent wear resistant superhydrophobic coatings[J].Materials Reports, 2020,34 (12):12005-12009.

[35] Russell T, Dinariev O Y, Pessoa Rego L A, et al. Averaged Boltzmann's kinetics for colloidal transport in porous media[J]. Water Resources Research, 2021, 57(3): e2020WR029557.

[36] Movahedi H, Shaygan K, Bovet N, et al. Fate and cotransport of Pb (II) and Cd (II) heavy ions with bentonite colloidal flow in saturated porous media: The role of filter cake, counter ions, colloid concentration, and fluid velocity[J]. Journal of Hazardous Materials, 2024, 466: 133546.

[37] Wang M, Gao B, Tang D. Review of key factors controlling engineered nanoparticle transport in porous media[J]. Journal of hazardous materials, 2016, 318: 233-246.

[38] Movahedi H, Shaygan K, Bovet N, et al. Fate and cotransport of Pb (II) and Cd (II) heavy ions with bentonite colloidal flow in saturated porous media: The role of filter cake, counter ions, colloid concentration, and fluid velocity[J]. Journal of Hazardous Materials, 2024, 466: 133546.

[39] Z. Lu, A. Rath, S.H. Amini, A. Noble, S. Shahab， A computational fluid dynamics investigation of a novel flooded-bed dust scrubber with vibrating mesh.Int. J. Min. Sci. Technol., 32 (2022), pp. 525-537.

[40] Q. Liu, W. Nie, Y. Hua, et al.Research on tunnel ventilation systems: dust diffusion and pollution behaviour by air curtains based on CFD technology and field measurement[J].Build Environ, 147 (2019), pp. 44-60

[41] W. Nie, X. Zhang, H.T. Peng, et al. Research on air curtain dust control technology for environmental protection at fully mechanized working faces. Environmental Science and Pollution Research, 2022. In Press. DOI:10.1007/s11356-022-18775-1.